Article

Neuron

Comprehensive Characterization of the Major Presynaptic Elements to the *Drosophila* OFF Motion Detector

Highlights

- All *Drosophila* OFF motion pathway Tm cells are activated by brightness decrements
- None of the four cell types are direction selective
- Tm1, Tm2, Tm4, and Tm9 display a variety of temporal filter properties
- The four Tm cells are involved in OFF motion processing to different degrees

Authors

Etienne Serbe, Matthias Meier, Aljoscha Leonhardt, Alexander Borst

Correspondence

serbe@neuro.mpg.de (E.S.), mmeier@neuro.mpg.de (M.M.)

In Brief

Serbe et al. use calcium imaging, electrophysiology, and behavior to assess the roles of columnar elements in the OFF motion vision pathway of *Drosophila*. Here, the complex interaction of four cell types shapes the flies' responses to motion stimuli.

Serbe et al., 2016, Neuron *89*, 1–13
February 17, 2016
http://dx.doi.org/10.1016/j.neuron.2016.01.006

CellPress

Please cite this article in press as: Serbe et al., Comprehensive Characterization of the Major Presynaptic Elements to the *Drosophila* OFF Motion Detector, Neuron (2016), http://dx.doi.org/10.1016/j.neuron.2016.01.006

Neuron
Article

Comprehensive Characterization of the Major Presynaptic Elements to the *Drosophila* OFF Motion Detector

Etienne Serbe,[1,2,*] Matthias Meier,[1,2,*] Aljoscha Leonhardt,[1] and Alexander Borst[1]
[1]Max-Planck-Institute of Neurobiology, Am Klopferspitz 18, 82152 Martinsried, Germany
[2]Co-first author
*Correspondence: serbe@neuro.mpg.de (E.S.), mmeier@neuro.mpg.de (M.M.)
http://dx.doi.org/10.1016/j.neuron.2016.01.006

SUMMARY

Estimating motion is a fundamental task for the visual system of sighted animals. In *Drosophila*, direction-selective T4 and T5 cells respond to moving brightness increments (ON) and decrements (OFF), respectively. Current algorithmic models of the circuit are based on the interaction of two differentially filtered signals. However, electron microscopy studies have shown that T5 cells receive their major input from four classes of neurons: Tm1, Tm2, Tm4, and Tm9. Using two-photon calcium imaging, we demonstrate that T5 is the first direction-selective stage within the OFF pathway. The four cells provide an array of spatiotemporal filters to T5. Silencing their synaptic output in various combinations, we find that all input elements are involved in OFF motion detection to varying degrees. Our comprehensive survey challenges the simplified view of how neural systems compute the direction of motion and suggests that an intricate interplay of many signals results in direction selectivity.

INTRODUCTION

Extracting the direction of visual motion is an essential operation for most animals to successfully perform tasks like navigation, prey capture, predator avoidance, and mating. Correlation-type motion detectors represent a class of algorithmic models that achieve direction selectivity by multiplying signals from two adjacent photoreceptors after asymmetric temporal filtering (Figure 1A; Hassenstein and Reichardt, 1956). In various vertebrate and invertebrate species, this is realized separately for brightness increments (ON) and decrements (OFF; Werblin and Dowling, 1969; Joesch et al., 2010; Borst and Euler, 2011). In the mouse retina, for example, direction selectivity in OFF-type starburst amacrine cells is proposed to arise from spatially offset bipolar cell input (Kim et al., 2014). These cells exhibit temporally diverse calcium (Baden et al., 2013) and glutamate release signals (Borghuis et al., 2013). In *Drosophila melanogaster*, photoreceptor signals are processed in a retinotopic way within the four neuropils of the optic lobe, called lamina, medulla, lobula, and lobula plate (Figure 1B). In the lobula plate, wide-field tangential cells respond to motion stimuli in a fully opponent, direction-selective manner: they depolarize to motion along their preferred direction (PD) and hyperpolarize to motion along the opposite or null direction (ND; Joesch et al., 2008; Schnell et al., 2010). Tangential cells receive excitatory cholinergic input from two types of neurons, called T4 and T5 cells (Mauss et al., 2014). They were first described via Golgi stainings (Cajal and Sánchez, 1915) and exist in four subtypes, depending on their projection layer in the lobula plate (Figure 1B; Fischbach and Dittrich, 1989). Genetically silencing both cell types turns tangential cells motion insensitive and walking flies motion blind (Schnell et al., 2012; Bahl et al., 2013). Each of the four subtypes responds only to either brightness increments (ON for T4) or decrements (OFF for T5), moving in one of the four cardinal directions (front to back, back to front, upward, and downward). Blocking either T4 or T5 results in selectively diminished responses of lobula plate tangential cells to ON and OFF stimuli, respectively (Maisak et al., 2013). The splitting of ON and OFF signals starts at the level of lamina monopolar cells, which receive direct input from photoreceptors. L1 signals feed into the ON pathway; L2–L4 signals feed into the OFF pathway (Joesch et al., 2010, 2013; Clark et al., 2011; Eichner et al., 2011; Takemura et al., 2011; Silies et al., 2013; Meier et al., 2014). Electron microscopy reconstructions identified the primary interneurons that connect lamina monopolar cells to the dendrites of T4 and T5 cells. L1 synapses mainly onto the medulla intrinsic neuron Mi1 and onto the transmedulla neuron Tm3, which both contact T4 cells (Takemura et al., 2013). In the OFF pathway, reciprocally connected L2 and L4 cells (Rivera-Alba et al., 2011) connect to Tm1, Tm2, and Tm4 cells while L3 cells synapse onto Tm9 cells (Figure 1B; Takemura et al., 2013). These four Tm cells have been described as cholinergic and collectively account for nearly 90% of T5 input synapses, with Tm2 being the numerically dominant input (~33%), followed by Tm9 (~22%), Tm1 (~20%), and Tm4 (~13%; Takemura et al., 2011; Shinomiya et al., 2014). Calcium imaging and electrophysiological recordings revealed that Tm1 and Tm2 respond to OFF stimuli with transient activation, independent of the direction of motion (Meier et al., 2014; Strother et al., 2014; Behnia et al., 2014). Their dynamic properties, estimated using a white-noise stimulus, revealed an offset in peak response times of 13 ms. This led to the suggestion that Tm1 and Tm2 cells form the

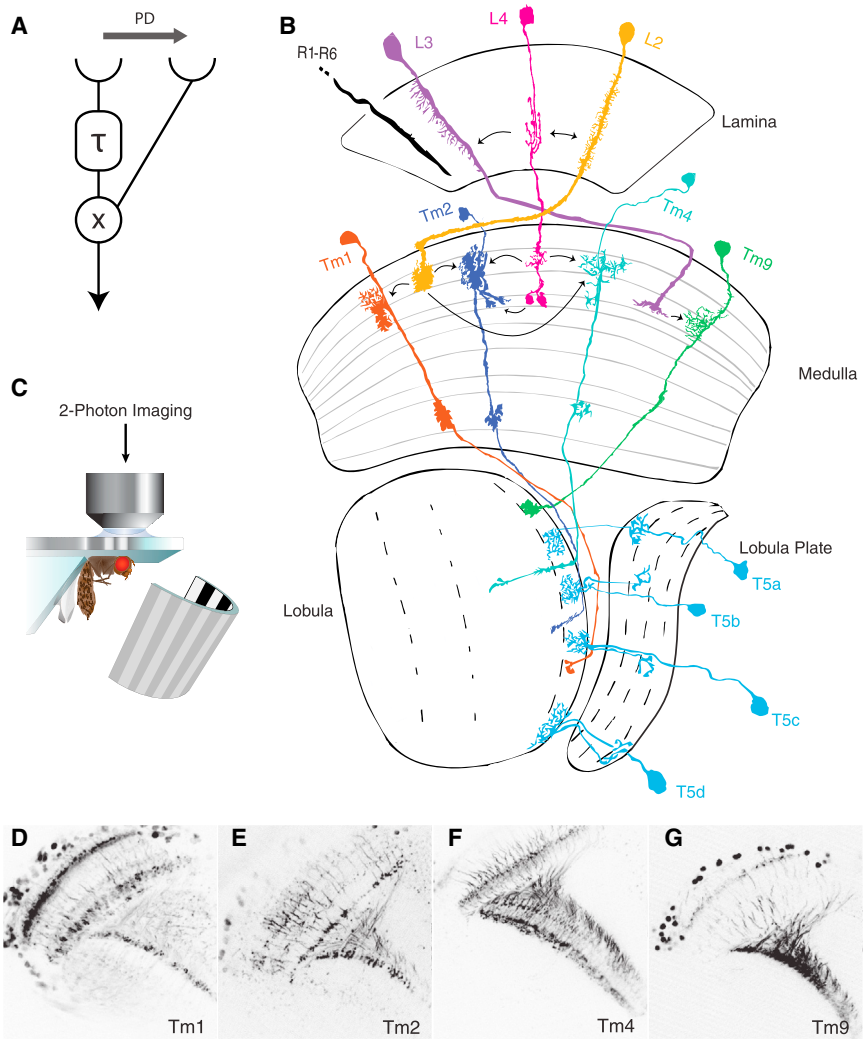

Figure 1. The OFF Pathway of *Drosophila* Motion Vision

(A) Schematic representation of a subunit of a Hassenstein-Reichardt correlator tuned to rightward motion (preferred direction, PD). Signals from two spatially offset inputs are multiplied (×) after one of them has been temporally delayed by a low-pass filter with the time constant τ.

(B) Wiring diagram of the proposed OFF pathway neurons. Photoreceptors R1–R6 project onto interconnected lamina monopolar cells L2 (yellow), L3 (purple), and L4 (magenta). The L2–L4 subpathway consists of transmedullary neurons Tm2 (dark blue) and Tm4 (cyan). L3 contacts Tm9 cells (green). Tm1 (orange) only receives input via L2 (yellow). All four Tm cells project into the lobula, giving input to the four subtypes of T5 (light blue). Arrows indicate synaptic contacts between cell types. (Modified from Fischbach and Dittrich, 1989.)

(C) Experimental setup for two-photon calcium imaging.

(D–G) Contrast-inverted maximum intensity z projections of two-photon image stacks through the optic lobe of flies expressing GCaMP6f in Tm1 (D), Tm2 (E), Tm4 (F), and Tm9 (G) cells.

two input lines of an OFF elementary motion detector (Behnia et al., 2014). Indeed, blocking Tm2 cells strongly reduces the responses of tangential cells to moving dark edges (Meier et al., 2014). Whether Tm1 is equally critical has not been clarified; neither have the roles of the other two input neurons, Tm4 and Tm9. We therefore set out to explore the response properties and necessity of all four major inputs to T5 cells, which constitutes a crucial step toward a mechanistic understanding of how direction selectivity is computed in the OFF pathway of *Drosophila*.

First, we performed two-photon calcium imaging (Figure 1C) to assess the visual response properties of all major T5 inputs, including direction selectivity, response dynamics, and receptive fields. Second, we blocked the synaptic output of single-cell types, as well as combinations of two-cell types, using *shibire*^{ts} (Kitamoto, 2001) and analyzed responses of tangential cells and walking flies to visual motion stimuli. Our results demonstrate that all four Tm cell types are activated by brightness decrements, irrespective of the direction of motion, confirming the notion that T5 cells are the first direction-selective cells within the OFF pathway (Maisak et al., 2013; Fisher et al., 2015). Their responses revealed substantially different temporal dynamics. Blocking their synaptic output individually and in combination exclusively impaired OFF motion vision, though by different magnitudes. Combinatorial blocking of two Tm cell types resulted in an increased reduction of the OFF motion response. These data do not map easily onto classical models of motion detection involving two input lines. Instead, they suggest a complex interplay of multiple inputs that finally generates direction selectivity.

RESULTS

Response Properties of Tm1, Tm2, Tm4, and Tm9 Cells

To directly examine the response properties of Tm cells, we expressed calcium indicator GCaMP5 (Akerboom et al., 2012) under the control of cell-type-specific Gal4 lines (Brand and Perrimon, 1993). We manually chose regions of interest that corresponded to single axonal terminals in the lobula where T5 dendrites are located (Figures 1D–1G) and determined the fluorescence change during visual stimulation. First, we characterized the calcium responses of T5's presynaptic elements by presenting edges of both polarities (ON and OFF edges) moving in the four cardinal directions. With these visual stimuli, we addressed two questions: First, are neurons upstream of T5 cells direction selective? Second, do they exhibit rectified responses with respect to the contrast polarity of the stimulus? In agreement with previous studies (Meier et al., 2014; Strother et al., 2014; Behnia et al., 2014), we found that Tm1 and Tm2 cells

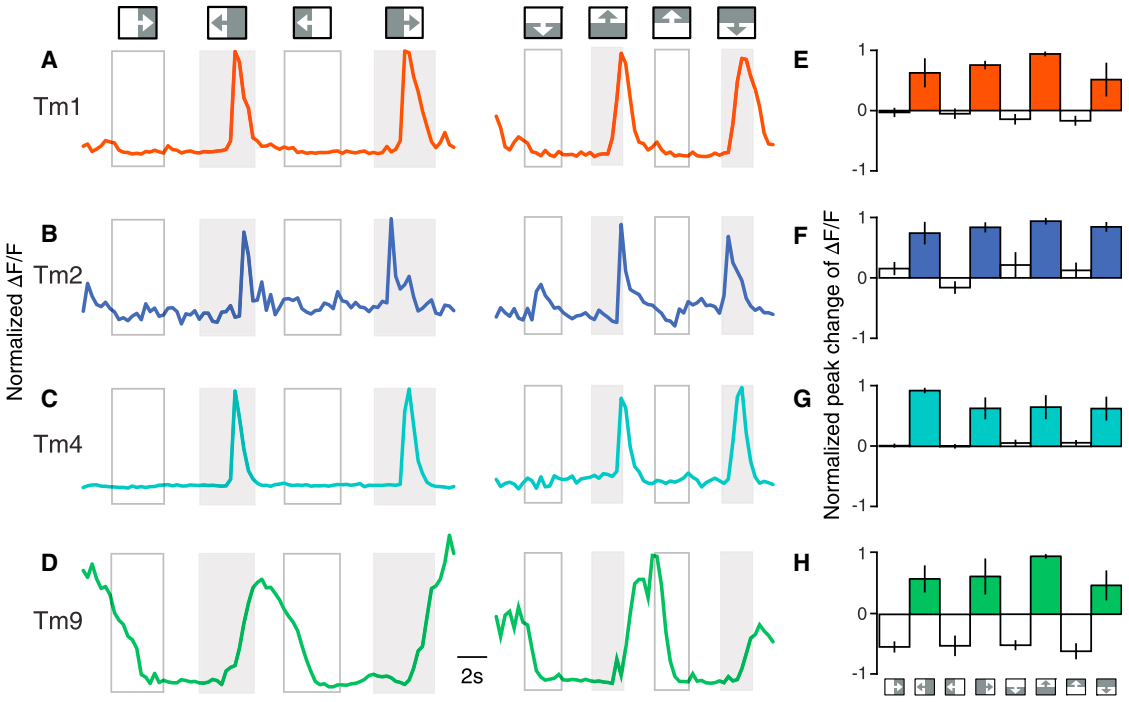

Figure 2. OFF Edges Activate Tm Cells Irrespective of the Direction of Motion

(A–D) Normalized ΔF/F calcium responses of single Tm1 (A), Tm2 (B), Tm4 (C), and Tm9 (D) cells. Flies were visually stimulated with ON and OFF edges moving horizontally (left panel) and vertically (right panel). Empty boxes indicate stimulation periods of ON edge motion; gray boxes indicate stimulation periods of OFF edge motion. Directions and polarity of edge motion are illustrated by little boxes on top. Between stimulations, luminance levels remain constant; i.e., after presentation of OFF edges, the stimulation device remains dark until the subsequent ON stimulus. After presentation of ON edges, the arena remains bright.

(E–H) Average normalized peak changes in calcium signals during edge presentation. Stimuli are represented at the bottom of (H). Tm1 (E; n = 11 cells in N = 11 flies), Tm2 (F; n = 8, N = 8), Tm4 (G; n = 9, N = 9), and Tm9 (H; n = 8, N = 8). Error bars indicate ± SEM.

See also Figure S7.

respond to moving brightness decrements (OFF edges) with a transient increase in calcium, independent of the direction of motion. In this experiment, neither Tm1 nor Tm2 cells showed any response when stimulated with moving brightness increments (ON edges; Figures 2A and 2B). Tm4 cells exhibited similar characteristics with short increases of activity when stimulated with OFF edges moving along all four cardinal directions (Figure 2C). The calcium levels of Tm9, however, changed more tonically, inversely following the local luminance level: when presented with a moving ON edge, the cell's initial calcium level dropped, and it only increased when a dark edge was moved through the fly's visual field (Figure 2D). Again, this was true for all four directions. To quantify the calcium responses to moving edges—and to detect increases, as well as decreases—we calculated the extremum (maximum or minimum) of the derivative of the fluorescence change for each stimulus (Figures 2E–2H). This demonstrated that all transmedullary neurons, anatomically identified to be presynaptic to T5, are not themselves direction selective and respond with increased activity to visual stimulation with dark edges. The response kinetics of the different Tm cells, however, looked qualitatively different. To more precisely characterize the temporal properties of Tm cells and to investigate whether the four cell types exhibit rectified responses with respect to contrast polarity, we increased the temporal resolution of the scanning microscope from 1.8 to 480 Hz by acquiring data from a single line through one axonal arbor in the lobula. Moreover, we expressed a faster calcium indicator, GCaMP6f (Chen et al., 2013), in the Tm cells. We used a 4.5°-wide, dark, vertical bar appearing and disappearing on a bright background for seven durations (50, 75, 125, 225, 425, 825, and 1,625 ms). All four Tm cells responded with an increase in calcium levels to local brightness decrements (Figures 3A–3D). Consistent with the edge stimulation results, this set of experiments revealed a broad range of response kinetics for the four Tm cell types. Furthermore, we observed a drop in calcium signaling upon stimulus offset. Based on these observations, we simulated their responses by fitting a three-stage filter model to the mean calcium traces (Figure 3E). Within this model, inputs were first linearly high-pass filtered (τ_{HP}), then rectified by setting negative values to zero, and finally low-pass filtered (τ_{LP}). Using this simple model, we were able to reproduce the measured calcium dynamics and estimate filter time constants for each cell type from the observed responses (Figures 3F–3I). In agreement with the data from the stimulation with moving edges, the four cell types could be classified in three groups: fast, transient Tm2 (τ_{HP} = 0.36 s and τ_{LP} = 0.1 s; Figures 3B and 3G) and Tm4 (τ_{HP} = 0.25 s and τ_{LP} = 0.2 s; Figures 3C and 3H), intermediate Tm1 (τ_{HP} = 1.23 s and τ_{LP} = 0.23 s; Figures 3A and 3F), and tonic Tm9 (τ_{LP} = 0.63 s; Figures 3D and 3I). In contrast to the other cell types, the slow dynamics of Tm9 responses were best predicted

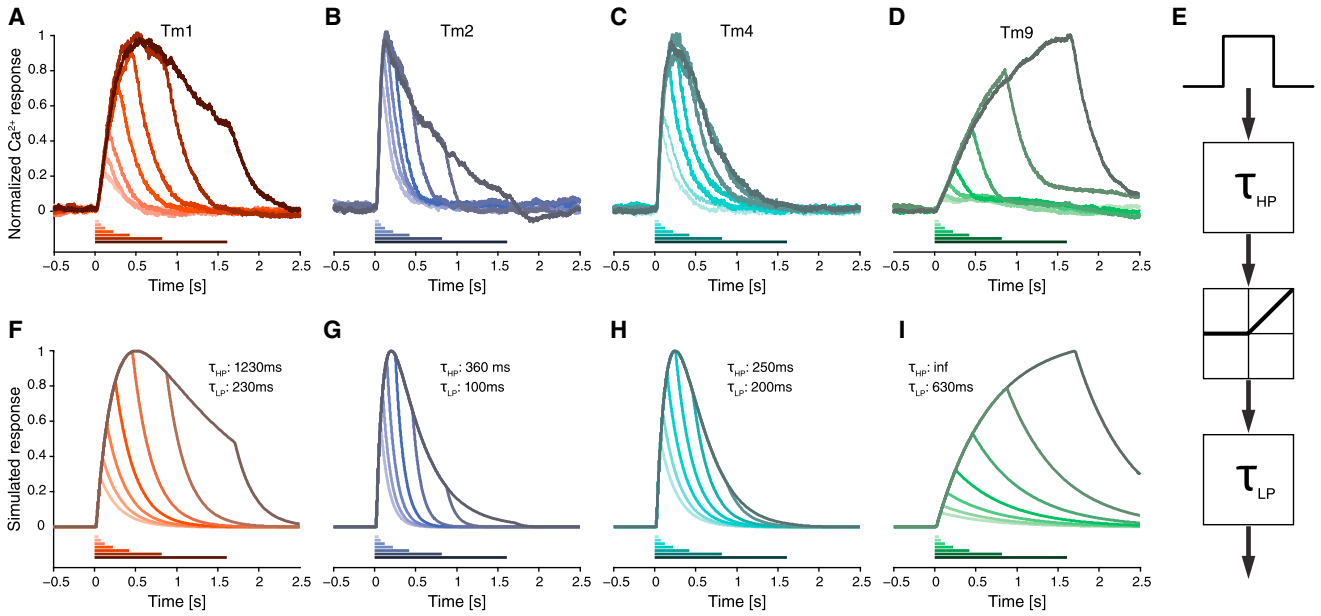

Figure 3. Temporal Tm Cell Response Properties

(A–D) Normalized ΔF/F calcium responses of Tm1 (A; n = 32, N = 5), Tm2 (B; n = 38, N = 5), Tm4 (C; n = 26, N = 3), and Tm9 (D; n = 44, N = 4), obtained by line scans through individual axonal arbors. Flies were presented with a 4.5°-wide, dark, vertical bar appearing on a bright background for seven periods: 50, 75, 125, 225, 425, 825, and 1,625 ms. Color-coded bars at the bottom of the graphs indicate the duration of stimulus presentation.

(E) Simulation procedure. The input signals were high-pass filtered (τ_{HP}), rectified, and low-pass filtered (τ_{LP}). Filter time constants are indicated in each panel.

(F–I) Simulated responses of Tm1 (F), Tm2 (G), Tm4 (H), and Tm9 (I) obtained by using the indicated time constants for the low-pass and high-pass filtering. For Tm9, no high-pass filtering was applied.

See also Figures S1 and S7.

by a pure low-pass filter. Also, prolonging the period of stimulus presentation to 2 and 4 s supported the finding that Tm9 cells respond tonically to visual stimulation with dark bars (Figure S1). To exclude that calcium buffering caused the slow dynamics of the Tm9 responses, we repeated the experiments using flies heterozygous for Gal4 and upstream activating sequence (UAS)-GCaMP6f to reduce expression levels of GCaMP. Here, we obtained the same results. In summary, the preceding results demonstrate that Tm1, Tm2, Tm4, and Tm9 are directionally unselective and thus confine the computation of direction selectivity in the OFF pathway to the dendrites of T5 cells. Furthermore, our data indicate that Tm cells provide a variety of temporal filters, ranging from fast, transient Tm2 and Tm4 over intermediate Tm1 to slow and sustained Tm9 cells.

Receptive Field Characteristics of Tm1, Tm2, Tm4, and Tm9

Current models for motion detection are based on the spatio-temporal correlation of input signals. It is thus crucial to characterize receptive field sizes and spatial integration properties of columnar neurons. To probe the receptive fields of the four Tm cells, we recorded changes in fluorescence at a lower temporal resolution of 1.8 Hz. Because our previous experiments (Figures 2 and 3) had revealed that all four cell types respond to changes in local luminance, we stimulated flies with 4.5°-wide, dark, vertical bars flickering on a bright background with 0.5 Hz at different azimuthal positions, each shifted by 1.5°. All four Tm cells tested with this stimulus exhibited similar receptive field sizes, ranging from 4.2° to 5.5° of half-width (Figures 4A–4E). We next used horizontal bars and presented them at different elevations. Again, we found comparable receptive field sizes with half-widths between 3.9° and 4.2° (Figure 4E). From this, we conclude that Tm1, Tm2, Tm4, and Tm9 cells have small isotropic receptive fields. The size of the measured receptive fields approximately corresponded to the visual acceptance angle of one neuro-ommatidium (Götz, 1964; Land, 1997), which indicates that the main activation of Tm cells is restricted to visual information detected by only one ommatidium. Stimulating the fly's eye in consecutive steps along the azimuth with terminals of several adjacent Tm9 cells in focus nicely revealed the retinotopic organization of columnar elements projecting from the medulla to the lobula (Movie S1). Next, we investigated spatial integration properties by centering a flickering dark, vertical bar at the position of maximal excitability of individual Tm cells. After each period of stimulation, we increased the width of the bar. All four cell types showed maximum responses when stimulated with bars of a 4.5° to 7.5° width but decreased activity when presented with stimuli spanning larger areas in visual space (Figures 4F–4I). Hence, all cells seem to be subject to lateral inhibition, preventing them from responding to wide-field flicker. The responses of Tm9 cells diverged from the other cell types for full-field stimulation (180° azimuth): while the calcium response levels elicited by flicker between a 13.5° and a 67.5° width were small, the response to full-field darkening amounted

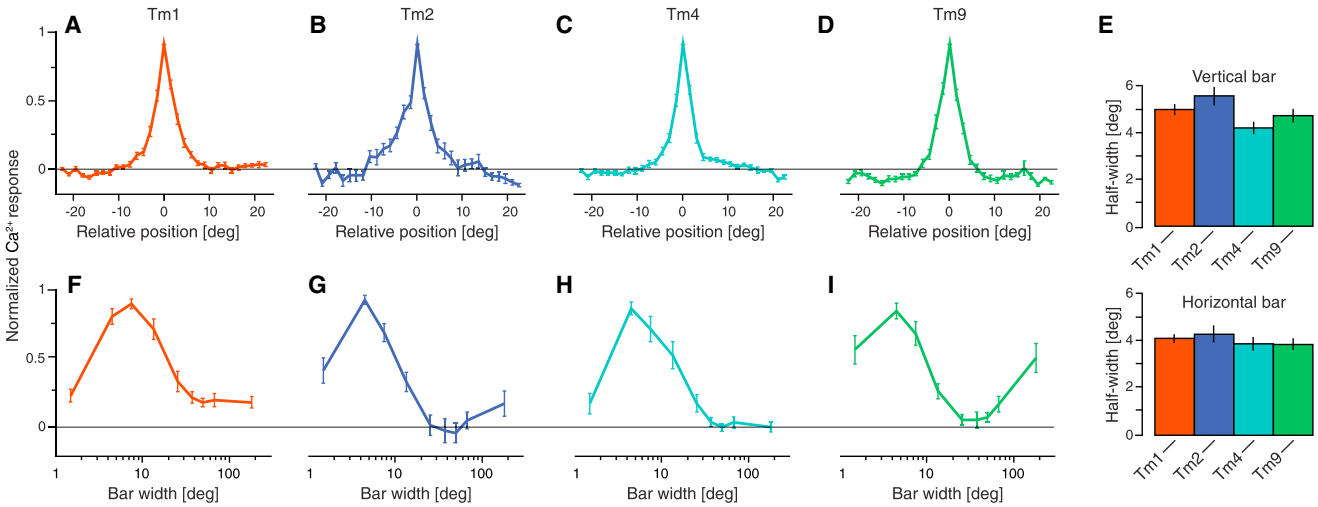

Figure 4. Receptive Field Properties of Tm Cells

(A–D) Spatial receptive fields measured by normalized calcium responses of Tm1 (A; n = 45, N = 10), Tm2 (B; n = 29, N = 8), Tm4 (C; n = 30, N = 5), and Tm9 (D; n = 31, N = 8) to 4.5°-wide, dark, vertical bars appearing and disappearing at various positions (shifted by 1.5°) on a bright background at a frequency of 0.5 Hz.

(E) Quantification of receptive field half-width for vertical bars (top panel) and horizontal bars (bottom panel). Tm1 (n = 37, N = 8), Tm2 (n = 26, N = 6), Tm4 (n = 20, N = 3), and Tm9 (n = 24, N = 3).

(F–I) Spatial integration properties measured by normalized calcium responses of Tm1 (F; n = 15, N = 9), Tm2 (G; n = 16, N = 7), Tm4 (H; n = 9, N = 4), and Tm9 (I; n = 9, N = 4) to dark, vertical bars of increasing size (bar widths: 1.5°, 4.5°, 7.5°, 13.5°, 25.5°, 37.5°, 49.5°, 67.5°, and 180°).

Error bars indicate ± SEM. See also Figure S7.

to approximately 50% of the maximum response. Tm9 has been shown to receive its main synaptic inputs through a different set of neurons from those for Tm1, Tm2, and Tm4 (L3 for Tm9, compared to L2 for Tm1, Tm2, and Tm4; Takemura et al., 2013). Together with the particular spatial integration property, the anatomical distinctness of Tm9 suggests that lateral inhibition could be implemented by two different mechanisms in the OFF pathway. Taken together, using calcium levels as a proxy for neuronal activity, we established that Tm1, Tm2, Tm4, and Tm9 are small-field columnar neurons that receive isotropic lateral inhibition.

Blocking OFF Pathway Tm Cells Reduces Responses of Lobula Plate Tangential Cells Specifically to OFF Edges

The response properties of *Drosophila* lobula plate tangential cells have been well characterized using various visual stimuli (Joesch et al., 2008, 2010; Schnell et al., 2010; Mauss et al., 2015). Furthermore, these large-field interneurons have been demonstrated to receive excitatory input from T4 and T5 cells (Schnell et al., 2012; Mauss et al., 2014). Hence, responses of lobula plate tangential cells can be used as a readout to assess the contribution of presynaptic elements within the motion detection circuit (Joesch et al., 2010; Schnell et al., 2012; Maisak et al., 2013; Meier et al., 2014). We performed somatic whole-cell patch clamp recordings from tangential cells of the vertical system (VS) and horizontal system (HS) while blocking the output of different Tm cells. We stimulated flies with either multiple ON or OFF edges (Figure S7). Synaptic transmission was silenced by expressing temperature-sensitive *shibire^{ts}* (Pfeiffer et al., 2012) under the control of specific Gal4 driver lines. We confirmed the identities of cell types in the Gal4 lines by expressing GFP in a small subset of neurons using a flip-out approach (Figures 5A–5D; Nern et al., 2015). To increase block strength without a loss of expression specificity, we used flies with two copies of UAS-*shibire^{ts}* (shi^{ts}/shi^{ts}) and one copy of the Gal4 driver. Tangential cells of control flies responded with approximately equal strength to motion of bright or dark edges (Figures 5E–5H). We could thus use these stimuli to probe contrast-polarity-specific effects of Tm cell blocks. Based on the diversity of temporal response properties observed in our calcium imaging experiments reported earlier, we hypothesized that different Tm cell types may play distinct roles depending on motion velocity, as was recently shown for input elements to the ON direction-selective T4 cells (Ammer et al., 2015). We therefore tested flies using edges moving at nine velocities across two orders of magnitude (3.125°/s–800°/s; Figure S2). When Tm1 was removed from the circuit, lobula plate tangential cells responded only with about half of the magnitude of control flies to moving dark edges (Figures 5E and 5I). In agreement with a previous study, responses were strongly reduced when Tm2 was blocked (Meier et al., 2014). Both effects were present over all velocities tested (Figures 5F and 5J). Blocking Tm4 produced the weakest phenotype (Figures 5G and 5K). Interrupting Tm9 signaling resulted in the strongest effect of all cells tested and, as with the other cells, did so consistently across all stimulus velocities (Figures 5H and 5L). To our surprise, here, we did not find differential effects of blocking any of the four Tm cell types when using different edge velocities. To compare the overall effects of silencing single Tm cells, we calculated the average response relative to control flies over the whole range of stimulus velocities (Figures 5M–5P). Critically, in all silencing experiments, responses to ON edges were not significantly altered. Blocking

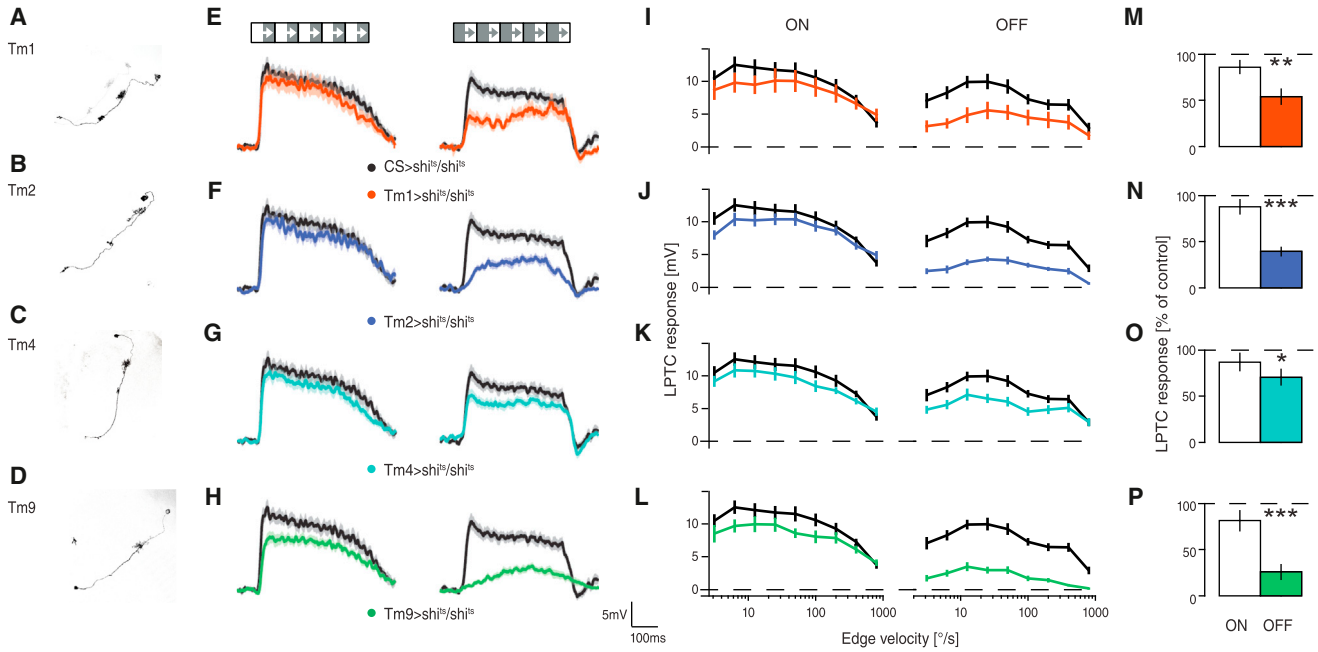

Figure 5. Blocking Tm Cells Impairs OFF Motion Vision

(A–D) Stochastic labeling of single Tm1 (A), Tm2 (B), Tm4 (C), and Tm9 (D) cells, showing the specificity of the Gal4 driver lines.

(E–H) Example traces of mean responses to motion along the PD minus the response to motion along the ND of lobula plate tangential cell (LPTC) responses upon stimulation with multiple ON (left) and OFF (right) edges (50°/s) in control CS > shi^{ts}/shi^{ts} (black), Tm1 > shi^{ts}/shi^{ts} (E), Tm2 > shi^{ts}/shi^{ts} (F), Tm4 > shi^{ts}/shi^{ts} (G), and Tm9 > shi^{ts}/shi^{ts} (H) flies. Stimulus presentation is indicated by the panels on top.

(I–L) Mean PD-ND LPTC responses of control (black), Tm1 (I), Tm2 (J), Tm4 (K), and Tm9 (L) block flies upon ON (left panel) and OFF edge (right panel) stimulation for nine velocities (3.125°/s, 6.25°/s, 12.5°/s, 25°/s, 50°/s, 100°/s, 200°/s, 400°/s, and 800°/s).

(M–P) Responses averaged over all nine velocities of Tm1 (M), Tm2 (N), Tm4 (O), and Tm9 (P) block flies plotted as percentages of the controls. Responses were obtained from HS and VS cells. Because no difference was detected, data from both cell types were pooled. CS > shi^{ts}/shi^{ts} data are from 13 cells (5 HS, 8 VS) in 5 flies, Tm1 block data are from 10 cells (3 HS, 7 VS) in 7 flies, Tm2 block data are from 14 cells (7 HS, 7 VS) in 7 flies, Tm4 block data are from 16 cells (5 HS, 11 VS) in 9 flies, and Tm9 block data are from 15 cells (3 HS, 12 VS) in 8 flies. In all four Tm cell blocks, ON responses are not significantly reduced in comparison to control flies. OFF responses, however, are reduced at different significance levels. *$p < 0.05$, **$p < 0.01$, ***$p < 0.001$, tested using two-tailed t tests against the controls. Error shades and error bars indicate ± SEM. See also Figures S2–S4 and S7.

any of the four Tm cell types specifically impaired the responses of lobula plate tangential cells to moving dark edges, irrespective of stimulus velocity. The magnitude of effects, however, covered a wide range, with strong phenotypes for Tm9 (25.69% ± 6.37% of control, mean ± SEM, n = 15 recordings, $p < 0.001$) and Tm2 (39.22% ± 4.50%, n = 14, $p < 0.001$), intermediate effects for Tm1 block (53.98% ± 8.33%, n = 10, $p < 0.01$), and a weak phenotype for silencing Tm4 (70.59% ± 8.41%, n = 16, $p < 0.05$).

Combinatorial Blocking of Tm Cells Increases OFF Edge Phenotypes

Tm cells could contribute in parallel or modularly to direction selectivity in T5. Combining two cell-specific Gal4 lines, thereby driving the expression of *shibire^{ts}* in two cell populations simultaneously, allowed us to investigate how different Tm cells interact. To detect potential synergistic effects, we decreased individual blocking strength by using flies with only one copy of *shibire^{ts}* (shi^{ts}/+). When we repeated the same experiment as described earlier, the tangential cell responses of Tm1 block flies to dark-edge stimulation were only reduced to 76.29% ± 7.88% (percent of control, n = 11, p = 0.18; Figures 6A and 6B) as opposed to 54% for two copies of *shibire^{ts}*. Blocking Tm2 with one copy of *shibire^{ts}* resulted in a response reduction to 69.13% ± 4.25% (n = 11, p = 0.07; Figures 6G and 6H), while blocking Tm4 cells did not result in a detectable reduction of tangential cell responses (89.17% ± 7.95%, n = 12, p = 0.50; Figures 6M and 6N). Only responses of Tm9 block flies to dark edges remained significantly different from those of control flies (51.39% ± 6.02%, n = 10, $p < 0.01$; Figures 6S and 6T), even with only one copy of *shibire^{ts}*. Overall, we found that the effect size was reduced while relative effects remained the same, with blocking Tm9 resulting in the strongest reduction of the OFF response, followed by Tm2, Tm1, and finally Tm4. This offered an opportunity to compare partial single-cell blocks with the combinations of two incompletely blocked classes of neurons. The images in Figure S3 provide an overview of the expression patterns of the six binary combinations of the four Tm cell types. Combining Tm9 with one of the other three cell types resulted in the strongest reductions of tangential cell responses to OFF edges (Figures 6E, 6J, and 6O–6R). All three Tm9 combinations decreased responses beyond what we had determined for the single Tm9 block. Furthermore, Tm1/Tm2 and Tm2/Tm4 blocks reduced the responses of lobula plate tangential cells to moving dark stimuli (Figures 6C, 6F, 6I, and 6L) compared to the isolated

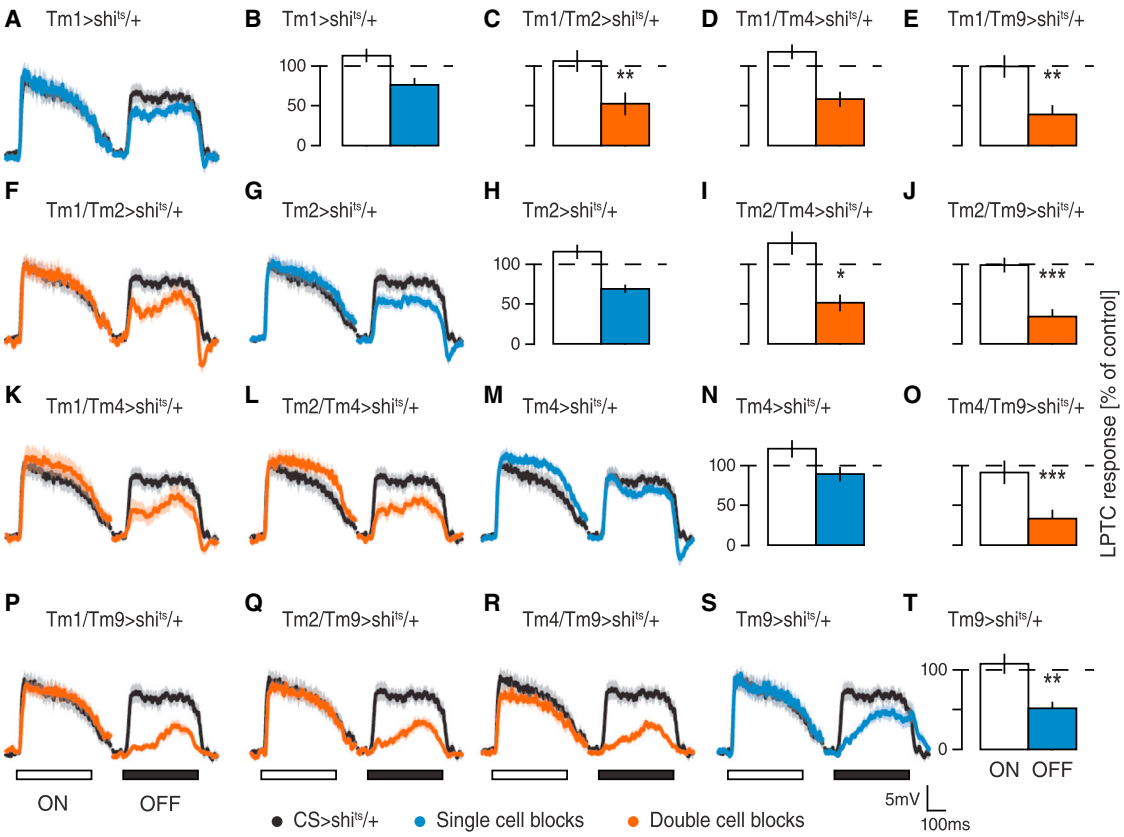

Figure 6. Combinatorial Blocking of Tm Cells

(A, F, G, K–M, and P–S) Mean traces of control (black), single-block (blue), and double-block (orange) flies for ON (left) and OFF (right) edge stimulation at a representative velocity of 50°/s.

(B–E, H–J, N, O, and T) Mean ON and OFF lobula plate tangential cell (LPTC) responses of single (blue) and double (orange) Tm cell block flies compared to control flies over nine velocities. Control CS > shi^{ts}/+ data are from 13 cells (5 HS, 8 VS) in 5 flies, Tm1 > shi^{ts}/+ data are from 11 cells (4 HS, 7 VS) in 6 flies, Tm2 > shi^{ts}/+ data are from 13 cells (6 HS, 7 VS) in 9 flies, Tm4 > shi^{ts}/+ data are from 12 cells (4 HS, 8 VS) in 6 flies, Tm9 > shi^{ts}/+ data are from 10 cells (3 HS, 7 VS) in 7 flies, Tm1/Tm2 > shi^{ts}/+ data are from 11 cells (3 HS, 8 VS) in 7 flies, Tm1/Tm4 > shi^{ts}/+ data are from 11 cells (4 HS, 7 VS) in 7 flies, Tm1/Tm9 > shi^{ts}/+ data are from 10 cells (3 HS, 7 VS) in 7 flies, Tm2/Tm4 > shi^{ts}/+ data are from 13 cells (3 HS, 10 VS) in 7 flies, Tm2/Tm9 > shi^{ts}/+ data are from 12 cells (4 HS, 8 VS) in 8 flies, and Tm4/Tm9 > shi^{ts}/+ data are from 10 cells (3 HS, 7 VS) in 7 flies. In all block flies, ON responses are not significantly reduced in comparison to control flies. OFF responses, however, are reduced at different levels. *$p < 0.05$, **$p < 0.01$, ***$p < 0.001$, tested using two-tailed t tests against the controls.

Error shades and error bars indicate ± SEM. See also Figures S3–S5 and S7.

Tm2 block. When the output of Tm1 and Tm4 was blocked simultaneously, we observed an intermediate reduction of tangential cell responses to OFF edges (Figures 6D and 6K). For all single- and double-block experiments with one copy of *shibire^{ts}*, responses to ON edges remained unaltered. Effects were consistent across all velocities tested for PD and ND stimulation (Figure S4). These results corroborate the conclusion drawn from single blocks, namely, that all four Tm cell types are involved in the detection of moving brightness decrements. Moreover, all combinatorial restrictions of two Tm cell outputs decreased OFF responses beyond the level of the respective single-cell blocks. To further investigate the effects of blocking T5 input elements on motion responses in tangential cells, we used square wave gratings (Figure S7) moving at eight temporal frequencies (from 0.07 to 8.89 Hz; Figure S5). In contrast to ON or OFF edges, square wave gratings did not allow for a specific stimulation of ON or OFF pathways. However, in contrast to a moving edge, they led to ongoing, permanent stimulation of local T5 motion-detecting cells, as well as their input neurons. The responses to square wave gratings were only mildly reduced. The reduction pattern, however, was similar to that for OFF edges (Figures S5A–S5N). Compared to controls (Figures S5O–S5X), it is apparent that responses to gratings in almost all blocking conditions decreased as temporal frequency increased. This effect can be explained through differentially tuned responses of lobula plate tangential cells to ON and OFF edges: tangential cells respond maximally to bright edges moving ~100 deg/s, whereas their responses to dark edges peak ~300 deg/s (Ammer et al., 2015). Hence, the ON channel appears to contribute more strongly to responses at lower frequencies. High frequencies seem to be mostly mediated through the OFF system. This asymmetry could thus account for the increased reductions in high-frequency regimes for the strongest OFF blocks (Figures S5R, S5S, S5U, S5W, and S5X).

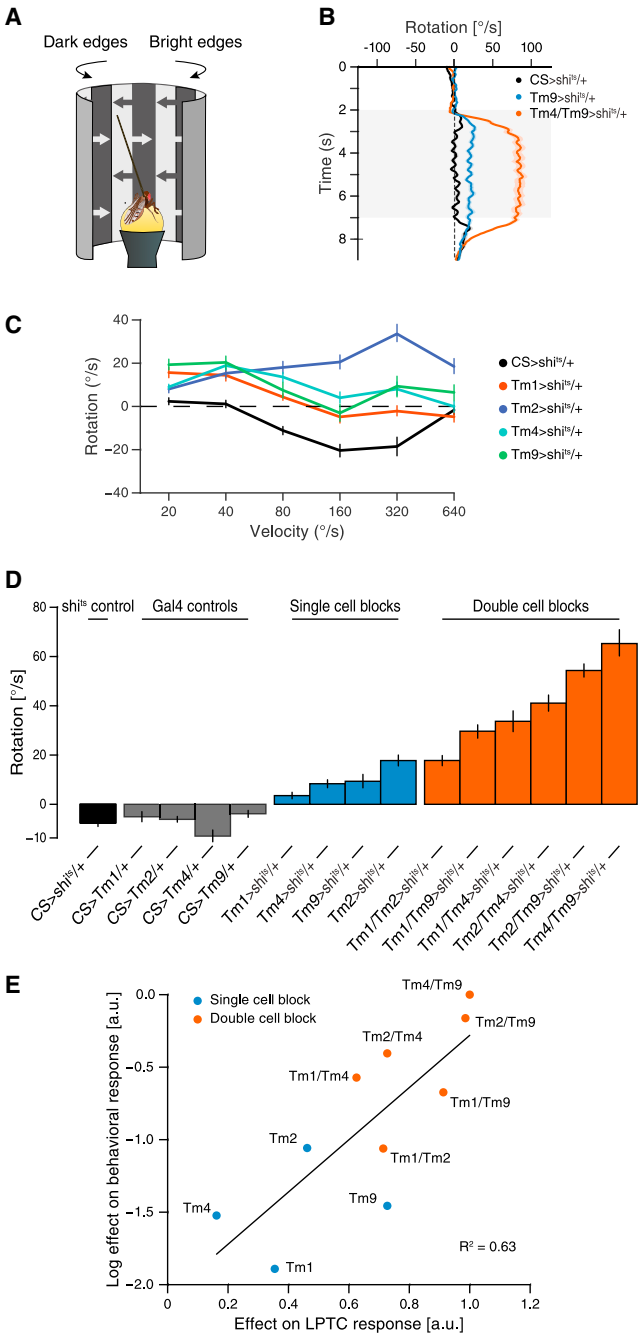

Figure 7. Blocking Tm Cells Affects Turning Behavior in Walking Flies

(A) Schematic illustration of the behavioral setup used in this study. A tethered fruit fly is walking on an air-suspended ball, facing a visual stimulation device. The fly is presented with a balanced motion stimulus (see Experimental Procedures).

(B) Exemplary optomotor responses of three genotypes to visual stimulation moving at 40°/s. Positive (rightward) rotation follows ON edges; negative (leftward) rotation follows OFF edges. Control flies do not exhibit any turning response for this velocity (black line), Tm9 block flies follow the bright edges with a low turning speed (blue line), and Tm4/Tm9 block flies turn with the direction of ON motion with a high angular velocity (orange line).

(C) Mean turning responses of control (black), Tm1 block (orange), Tm2 block (blue), Tm4 block (cyan), and Tm9 block (green) flies for stimulation with six velocities (20°/s, 40°/s, 80°/s, 160°/s, 320°/s, and 640°/s).

(D) Mean turning response of control (black and gray), single-block (blue), and double-block (orange) flies to stimulation with the balanced motion stimulus over all velocities tested. All blocking experiments were performed using one copy of *shibire*^{ts}. shi-control (N = 14), Tm1-control (N = 13), Tm2-control (N = 17), Tm4-control (N = 15), Tm9-control (N = 13). Tm1 (N = 12), Tm2-block (N = 13), Tm4-block (N = 13), Tm9-block (N = 12), Tm1/Tm2-block (N = 16), Tm1/Tm4-block (N = 12), Tm1/Tm9-block (n = 12), Tm2/Tm4-block (n = 16), Tm2/Tm9-block (n = 17), Tm4/Tm9-block (n = 14).

(E) Comparison of block effect strengths in the turning response of walking flies (y axis, log-transformed data) versus the effect of Tm cell blocks on the responses of lobula plate tangential cell (LPTCs; x axis, data not transformed). Single-cell blocks are colored in blue; double-cell blocks are in orange. The black line indicates a linear fit with $R^2 = 0.63$, indicating an exponential relationship between the behavioral effect and the reduction of the motion response as observed in the tangential cells. For details, see Experimental Procedures. Error shades and error bars indicate ± SEM. See also Figures S3, S6, and S7.

Blocking Tm Cells Affects Optomotor Responses in Walking Flies

The detection of visual motion is ultimately used to control behavior. The model proposed by Hassenstein and Reichardt (1956) was derived from quantitative observations of tethered walking beetles. To examine the effects of Tm cell blocks on the flies' turning responses during visual stimulation (Figure 7A), we monitored tethered *Drosophilae* walking on an air-suspended ball and repeated the blocking experiments as described earlier. We used multiple dark and bright edges, simultaneously moving in opposing directions (Clark et al., 2011). Compared to the direct measurement of optomotor responses to edge motion of a single polarity, this stimulus allows for a differential measurement of the flies' sensitivity to moving ON and OFF edges. Turning responses in walking and flying *Drosophilae* are not a direct readout of the membrane potential of lobula plate tangential cells (Schnell et al., 2014). Instead, signals are subject to leaky integration over a time window of multiple seconds. When examining responses, this may lead to robust behavioral responses despite strongly reduced lobula plate tangential cell signals. The opposing edge assay circumvents this issue by having edges of opposite polarities compete before the integration stage, such that small differences are amplified and become detectable at the level of turning responses. Critically, our electrophysiological experiments demonstrate that ON responses are generally not affected by blocking either of the four cells, suggesting that any imbalance we detect in behavior results from a defect specific to OFF motion processing.

At a stimulus velocity of 40°/s, control flies showed no turning response during presentation of opposing edges (Figure 7B), indicating that ON and OFF responses are intact and in balance. When we disrupted the output of either Tm9 or Tm4 and Tm9 in combination, block flies constantly followed the direction of moving ON edges (positive turning responses) with different amplitudes. This suggests an impairment of OFF motion detection at the behavioral level. When we used opposing edges moving at multiple velocities, control flies exhibited no turning response for slowly moving stimuli (20°/s and 40°/s) and started following dark edges (negative turning) when stimulated with patterns moving at higher speeds (80°/s–320°/s; Figures 7C and S6).

Turning behavior of Tm1, Tm4, and Tm9 block flies differed from control flies in a roughly constant way across all velocities, showing positive responses (following bright edges) for low velocities and no turning response for higher velocities. To our surprise, and in contrast to our electrophysiological data (Figure 5), we could see a velocity-dependent effect in Tm2 block flies, which followed the motion of bright edges more strongly at high velocities (Figure 7C). These data suggest that removing Tm2 from the circuit has comparatively little effect at low velocities but a pronounced effect at high velocities, suggesting a specialized role of Tm2 for processing of fast input signals.

To compare effects from electrophysiological recordings with the behavioral data, we averaged the turning response over all velocities tested (Figure 7D). On average, all control flies exhibit a small negative turning tendency that can be explained by the high-velocity stimuli where OFF signals dominate (Ammer et al., 2015; Figures 7C and S6). Blocking Tm2 with one copy of *shibire*^{ts} resulted in the strongest turning response, whereas flies with blocked Tm1 cells showed only weak turning responses syndirectional with bright edges. Tm4 and Tm9 block flies exhibited intermediate phenotypes. Hence, suppressing synaptic transmission in single Tm cell types resulted in phenotypes that resembled those of T5 block flies (Maisak et al., 2013) and were qualitatively comparable to the results obtained in electrophysiological experiments. Next, we looked at the turning responses of flies with combinations of two Tm cell types silenced. When we combined Tm9 with Tm4- or Tm2-specific driver lines, we observed the strongest effects, in accordance with our electrophysiological data (Figure 7D). For combinatorial blocks of Tm1/Tm9, Tm1/Tm4, and Tm2/Tm4, the behavioral response was increased compared to single blocks (Figure 7D). Only the combined block of Tm1 and Tm2 cells did not elicit a turning response stronger than that for the Tm2 block alone. To investigate the relation between behavioral and tangential cell responses, we plotted effects of single- and double-cell silencing observed in the tangential cell responses versus those observed in walking flies (Figure 7E). To compare positive measures of effect strength in behavior and electrophysiology, we subtracted the electrophysiological phenotypes (in percent of control) from 100 and normalized them via division by the strongest phenotype. We then normalized the behavioral effect in the same way. We found an interesting relationship between the response reduction at the level of lobula plate tangential cells and the behaviorally measured ON-OFF imbalance. This relation is well explained by an exponential fit (black line in Figure 7E), suggesting that the transformation of tangential cell responses into behavioral output is highly nonlinear. A saturating transfer function, for instance, would explain how small and intermediate block effects at the level of the lobula plate produce comparatively weak effects at the level of walking behavior. Only when lobula plate tangential cell activity is heavily suppressed do walking flies show strong deficiencies for dark-edge motion, as indicated by the opposing edge results. Given that lobula plate networks feed into complex post-synaptic cascades before controlling motor output, this is not surprising. Generally, our electrophysiological findings predicted the behavioral phenotypes well, lending further credence to our results and indicating that the reductions we see at the level of lobula plate tangential cells have direct impact on course control of behaving flies. Considering the combined dataset of tangential cell responses and behavior of walking flies, we conclude that all four Tm cells investigated here contribute to the computation of motion in the OFF pathway.

Reichardt Detector Simulations Using Tm Cells' Temporal Filters

A classical elementary motion detector (Hassenstein and Reichardt, 1956) consists of two spatially offset input lines that are multiplied after temporal filtering (Figure 1A). This is done in a mirror-symmetric fashion, and the outputs of the multiplication stages are subtracted from each other (insets in Figures 8A–8F). We used the calculated temporal filters of the Tm cells from Figures 3F–3I to simulate the responses of elementary motion detectors that are built from the six binary combinations of two Tm cells to grating stimulation (Figures 8A–8F). To obtain velocity tuning curves, we modeled responses to temporal frequencies ranging from 0.1 to 10 Hz (Figure 8). Except for the combination of Tm2 and Tm4, which have almost identical response dynamics, all Tm cell combinations led to direction-selective responses that varied in relative amplitude and tuning (Figures 8A–8F). Tuning curves of the four pairs Tm1/Tm2, Tm1/Tm4, Tm9/Tm2, and Tm9/Tm4 showed similar shapes and response amplitudes, peaking ~0.5 Hz. The Tm1/Tm9 model produced the strongest responses, peaking ~0.2 Hz. We calculated the mean of all detector outputs and normalized the tuning curve to compare the results with the physiological data (from Figure S5). The frequency tuning curves were largely similar, and both peaked ~0.5 Hz (Figure 8G). The shape of the tangential cell tuning curve, however, was wider than that of the simulation curve, which can be explained by saturation effects in tangential cells. From this, we conclude that the measured temporal response properties of all Tm cells are suitable for correlation-type elementary motion detectors.

DISCUSSION

In this study, we characterized the response properties of the four Tm cell types Tm1, Tm2, Tm4, and Tm9 and analyzed their involvement in *Drosophila* OFF motion detection. We demonstrated that none of these cells are direction selective and thus conclude that the computation of direction selectivity in the OFF pathway takes place on the dendrites of T5 cells.

At multiple levels, this circuit arrangement bears a striking resemblance to a network motif found in the mammalian retina (Kim et al., 2014). First, comparable to T5 cells, direction-selective starburst amacrine cells receive synaptic input from several anatomically similar cell types, i.e., the OFF bipolar cells 1, 2, 3a, 3b, and 4 (Masland, 2012). Second, like the Tm cells presynaptic to T5, these OFF bipolar cells have been shown to respond in a directionally unselective manner (Yonehara et al., 2013; Park et al., 2014). Third, the five OFF bipolar cell types show dynamics similar to those of the four Tm cells described here, ranging from sustained over slow decaying to fast transient (Baden et al., 2013; Borghuis et al., 2013). Depending on their temporal response properties, Tm cells receive input from particular groups of lamina monopolar cells. The two fast and transient

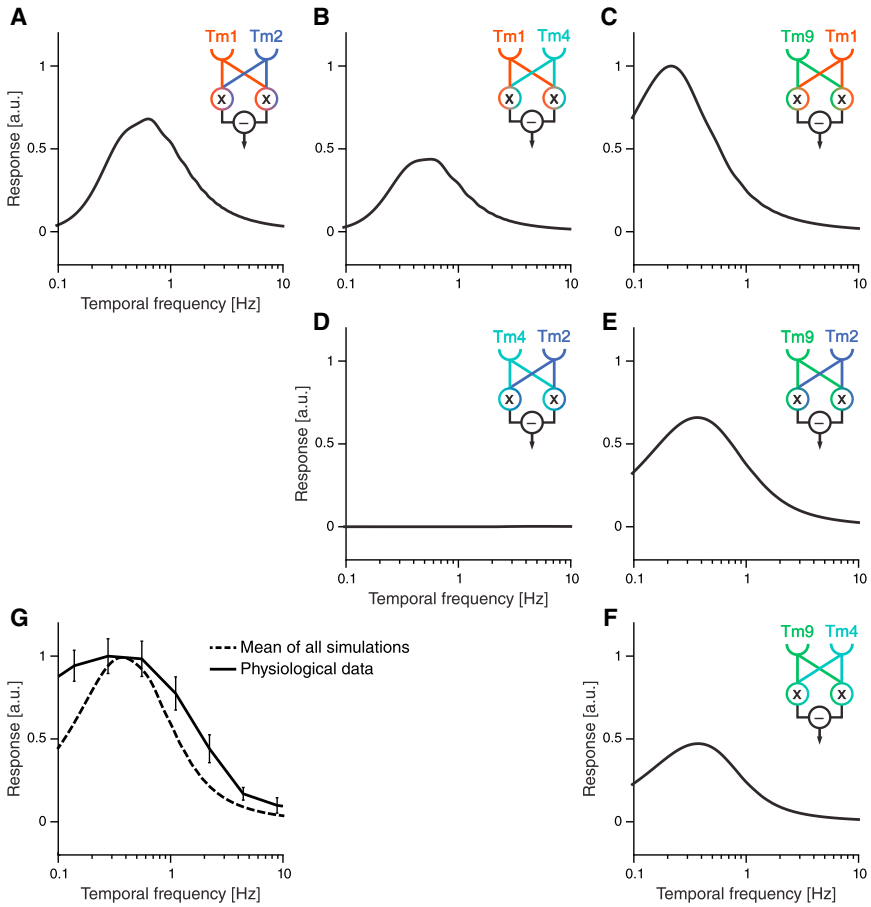

Figure 8. Simulated Frequency Tunings for the Six Combinations of Tm Cells

(A–F) Reichardt detector responses to grating stimulation using the simulated temporal filters (Figure 3) of Tm1/Tm2 (A), Tm1/Tm4 (B), Tm1/Tm9 (C), Tm2/Tm4 (D), Tm2/Tm9 (E), and Tm4/Tm9 (F). The responses were normalized to the maximal response of the Tm1/Tm9 detector (C).

(G) Comparison of the normalized mean response of all six simulations with the normalized physiological data of control flies (from Figure S5). Error bars indicate ± SEM.

See also Figure S5.

cells, Tm2 and Tm4, receive their major input from L2 and L4; intermediate Tm1 cells primarily receive input from L2; and tonic Tm9 cells receive input from similarly slow and sustained L3 (Clark et al., 2011; Freifeld et al., 2013; Silies et al., 2013; Takemura et al., 2013; Meier et al., 2014). Finally, the mechanism for the computation of direction selectivity on the dendrites of starburst amacrine cells has been proposed to rely on dendritically offset input from bipolar cells with different temporal filter properties (Kim et al., 2014). For T5, comparable spatial shifts among dendritic target sites of Tm1, Tm2, and Tm9 have been reported (Shinomiya et al., 2014). The aforementioned study, however, was not able to identify the preferred direction of corresponding T5 cells and thus could not correlate it with the particular arrangement of Tm cell input on the dendrite. Nevertheless, the remarkable resemblance of neural circuits between invertebrates and mammals suggests a universality of underlying computational principles (Borst and Helmstaedter, 2015).

Are the measured temporal response properties functionally relevant for the computation of direction-selective signals? We addressed this question by modeling six elementary motion detectors through filtering of the signals in the two neighboring arms with the time constants of all six possible binary combinations of Tm cells (Figure 8). Lobula plate tangential cells exhibit a maximal steady-state response when presented with square wave gratings moving at a temporal frequency of about 0.5 Hz (Figures 8G and S5). Except for Tm2/Tm4, whose filter time constants are almost identical, all combinations resulted in frequency optima in a range compatible with tangential cell responses. Furthermore, the mean signal of all simulations matches the tuning curve of electrophysiologically measured responses well. These simulations only represent a simplified view. They do not take into account several important aspects, such as the temporal frequency tuning of the ON channel, the different synaptic weights, or any spatial offsets of Tm cells on the T5 dendrites. Nevertheless, this simple model confirms the functional plausibility of the time constants of the four Tm cells tested.

We also demonstrated that the functional importance of each of the four Tm cell types correlates with the number of synaptic contacts to T5 (Shinomiya et al., 2014). Silencing Tm4 cells, which out of the four provide the smallest number of synapses onto T5 cells, resulted in the weakest phenotype, followed by Tm1. Blocking Tm2 and Tm9, numerically the strongest inputs to T5, produced the strongest impairment of the OFF response (Figures 5 and 7). However, silencing L3, which is thought to be the main input to Tm9, does not result in similar, purely OFF-specific effects (Silies et al., 2013; Tuthill et al., 2013). This can be due to two facts. First, L3 also strongly connects to crucial ON pathway element Mi1 (Takemura et al., 2013; Ammer et al., 2015). Second, additional inputs to Tm9 cells may influence their response properties.

Given the increased effects of impairment when blocking pairs of Tm cells, we are able to rule out complete redundancy of individual elements (Figures 6 and 7). How do these four cell types then map onto the elements of correlation-type models? First, the interaction of several Tm cell types may give rise to a nonlinear stage more complex than the simple multiplication in the Hassenstein-Reichardt correlator. It is conceivable that the biophysical implementation of a suitable nonlinearity requires more than two appropriately tuned input lines. Our behavioral data lend some support to this hypothesis, because the

strongest combinatorial blocks display a supra-linear increase in effect strength compared to the sum of the single-cell effects (Figure 7E). Second, standard algorithms generally model the asymmetric processing of direct and delayed lines as single-stage linear filters. For biophysical realizations, this filtering may be more complex. Multiple cells with varying intrinsic membrane properties and different synaptic transmission characteristics could provide many degrees of freedom when implementing filters that are appropriate for motion detection. Thus, temporal processing within one input line of the algorithmic model (Figure 1A) may involve the combination of two or more cells; Tm9 and Tm4, for instance, could both correspond to a module implementing what is the delay line in the Hassenstein-Reichardt model. Third, the four cells may in principle play different roles in different stimulus regimes defined by, for instance, velocity, contrast, luminance, or color. Our results provide some evidence for such a division of labor. In walking flies, the velocity-dependent phenotype of Tm2 block flies, together with the cells' fast response characteristics (Figure 3B), suggests a specific role for Tm2 at high velocities (Figure 7C). Such a design principle may be realized in at least two ways. Functional specialization could be a static property of the system, derived from cell-intrinsic spatiotemporal or chromatic filter properties, or a dynamic property that is subject to regulation depending on stimulus conditions. A recent study showed that changes in the behavior of hawkmoths under dim light conditions can be reproduced by adapting the filter time constants of a Hassenstein-Reichardt correlator (Sponberg et al., 2015). Tm9 could represent a candidate to detect changes in global luminance due to its slow filter properties, which make it sensitive to both brightness increments and decrements at all timescales (Figures 3D and 3I), as well as due to its responsiveness to full-field flicker (Figure 4I). Moreover, inputs from the color vision pathway have been demonstrated to improve motion discrimination (Wardill et al., 2012). Histaminergic photoreceptors R7 and R8, known to be involved in color perception (for review, see Behnia and Desplan, 2015), project to the medulla layers where Tm cell dendrites reside. Both Tm2 and Tm9 express a histamine-gated chloride channel (Gao et al., 2008), potentially linking the color and motion detection pathways. Finally, different Tm cells could be of different importance depending on the behavioral state of the animal, e.g., whether it is at rest, walking, or flying. Such behavioral-state dependency has been described at the level of the lobula plate tangential cells (Maimon et al., 2010; Chiappe et al., 2010; Haag et al., 2010; Jung et al., 2011; Schnell et al., 2014) and could be well explained by changes in contribution of synaptic input to T4 and T5 cells. Such a scenario could explain why blocking Tm2, Tm4, and their combinations resulted in stronger phenotypes in walking flies compared to tangential cell responses in a quiescent preparation (Figure 7E).

Taken together, our study sheds light on the circuitry underlying the computation of motion and uncovers striking parallels between vertebrate and invertebrate systems. Unraveling the exact mechanisms awaits further investigation. More naturalistic stimuli and modified algorithmic or biophysically realistic models that reflect the complexity of the neural correlate will play critical roles in this endeavor.

EXPERIMENTAL PROCEDURES

For calcium imaging, we used the genetically encoded indicators GCaMP5 (Akerboom et al., 2012) and GCaMP6f (Chen et al., 2013). Blocking experiments were accomplished using Tm cell-specific Gal4 lines crossed with pJFRC100-20XUAS-TTS-Shibire-ts1 (Pfeiffer et al., 2012) flies. Fly line specificity was tested using stochastic flip-out labeling (Nern et al., 2015) and expression of mCD8-GFP. All genotypes used in this study can be found in Table S1. Flies were prepared as described before: imaging experiments (Reiff et al., 2010), electrophysiology (Joesch et al., 2008), and behavior (Bahl et al., 2013). Two-photon microscopy and visual stimulus presentation was as described in Maisak et al. (2013). The recording protocol for electrophysiological experiments was adapted from Joesch et al. (2008). Under polarized light contrast, the glial sheet was digested locally by applying a stream of 0.5 mg/ml collagenase IV (Gibco) through a cleaning micropipette (~5 μm opening). Recordings for the blocking electrophysiology experiments were obtained within 2 hr after a 60 min heat-shock application at 37°C. For statistical analysis, we used a two-tailed t test to compare *shibire*^{ts} controls and block flies (*$p < 0.05$, **$p < 0.01$, ***$p < 0.001$). Behavioral experiments were conducted as previously described (Ammer et al., 2015). For immunostaining procedures, see Schnell et al. (2010). Data were evaluated offline using custom written software (Matlab and Python) and Origin (OriginLab). For modeling the time constants in Figure 3, we fit a three-stage filter model to the mean calcium traces. Within this model, inputs were first high-pass filtered, then rectified by setting negative values to zero, and finally low-pass filtered (Figure 3E). For the modeling results in Figure 8, we simulated grating responses of hypothetical Reichardt detectors whose inputs were band-pass filters as determined in Figure 3E. See Supplemental Experimental Procedures for detailed methods.

SUPPLEMENTAL INFORMATION

Supplemental Information includes Supplemental Experimental Procedures, seven figures, one table, and one movie and can be found with this article online at http://dx.doi.org/10.1016/j.neuron.2016.01.006.

AUTHOR CONTRIBUTIONS

E.S. and M.M. jointly performed and evaluated all calcium imaging and electrophysiology experiments. A.L. performed and evaluated the behavioral experiments. A.L. and A.B. performed computer simulations. A.B., E.S., and M.M. designed the study. E.S. and M.M. wrote the manuscript with the help of the other authors.

ACKNOWLEDGMENTS

We thank J. Haag for technical support and help with the two-photon microscope; R. Kutlesa and C. Theile for excellent help with behavior experiments; W. Essbauer, R. Kutlesa, C. Theile, and M. Sauter for fly work and immunostainings; T. Schilling for artwork; and D. Soll for the Dlg antibody. We thank G. Ammer, A. Arenz, J. Pujol-Marti, and A. Mauss for carefully reading the manuscript. All authors are members of the Graduate School for Systemic Neurosciences, Munich. We thank B. Dickson, G. Rubin, and A. Nern for providing us with unpublished fly lines.

Received: June 25, 2015
Revised: November 18, 2015
Accepted: December 18, 2015
Published: February 4, 2016

REFERENCES

Akerboom, J., Chen, T.-W., Wardill, T.J., Tian, L., Marvin, J.S., Mutlu, S., Calderón, N.C., Esposti, F., Borghuis, B.G., Sun, X.R., et al. (2012). Optimization of a GCaMP calcium indicator for neural activity imaging. J. Neurosci. *32*, 13819–13840.

Ammer, G., Leonhardt, A., Bahl, A., Dickson, B.J., and Borst, A. (2015). Functional specialization of neural input elements to the *Drosophila* ON motion detector. Curr. Biol. *25*, 2247–2253.

Baden, T., Berens, P., Bethge, M., and Euler, T. (2013). Spikes in mammalian bipolar cells support temporal layering of the inner retina. Curr. Biol. *23*, 48–52.

Bahl, A., Ammer, G., Schilling, T., and Borst, A. (2013). Object tracking in motion-blind flies. Nat. Neurosci. *16*, 730–738.

Behnia, R., and Desplan, C. (2015). Visual circuits in flies: beginning to see the whole picture. Curr. Opin. Neurobiol. *34*, 125–132.

Behnia, R., Clark, D.A., Carter, A.G., Clandinin, T.R., and Desplan, C. (2014). Processing properties of ON and OFF pathways for *Drosophila* motion detection. Nature *512*, 427–430.

Borghuis, B.G., Marvin, J.S., Looger, L.L., and Demb, J.B. (2013). Two-photon imaging of nonlinear glutamate release dynamics at bipolar cell synapses in the mouse retina. J. Neurosci. *33*, 10972–10985.

Borst, A., and Euler, T. (2011). Seeing things in motion: models, circuits, and mechanisms. Neuron *71*, 974–994.

Borst, A., and Helmstaedter, M. (2015). Common circuit design in fly and mammalian motion vision. Nat. Neurosci. *18*, 1067–1076.

Brand, A.H., and Perrimon, N. (1993). Targeted gene expression as a means of altering cell fates and generating dominant phenotypes. Development *118*, 401–415.

Cajal, S.R., and Sánchez, D. (1915). Contribución al conocimiento de los centros nerviosos de los insectos. Trab. Lab. Inv. Biol. *13*, 1–168.

Chen, T.W., Wardill, T.J., Sun, Y., Pulver, S.R., Renninger, S.L., Baohan, A., Schreiter, E.R., Kerr, R.A., Orger, M.B., Jayaraman, V., et al. (2013). Ultrasensitive fluorescent proteins for imaging neuronal activity. Nature *499*, 295–300.

Chiappe, M.E., Seelig, J.D., Reiser, M.B., and Jayaraman, V. (2010). Walking modulates speed sensitivity in *Drosophila* motion vision. Curr. Biol. *20*, 1470–1475.

Clark, D.A., Bursztyn, L., Horowitz, M.A., Schnitzer, M.J., and Clandinin, T.R. (2011). Defining the computational structure of the motion detector in *Drosophila*. Neuron *70*, 1165–1177.

Eichner, H., Joesch, M., Schnell, B., Reiff, D.F., and Borst, A. (2011). Internal structure of the fly elementary motion detector. Neuron *70*, 1155–1164.

Fischbach, K.-F., and Dittrich, A.P.M. (1989). The optic lobe of *Drosophila melanogaster*. I. A Golgi analysis of wild-type structure. Cell Tissue Res. *258*, 441–475.

Fisher, Y.E., Silies, M., and Clandinin, T.R. (2015). Orientation selectivity sharpens motion detection in *Drosophila*. Neuron *88*, 390–402.

Freifeld, L., Clark, D.A., Schnitzer, M.J., Horowitz, M.A., and Clandinin, T.R. (2013). GABAergic lateral interactions tune the early stages of visual processing in *Drosophila*. Neuron *78*, 1075–1089.

Gao, S., Takemura, S.-Y., Ting, C.-Y., Huang, S., Lu, Z., Luan, H., Rister, J., Thum, A.S., Yang, M., Hong, S.-T., et al. (2008). The neural substrate of spectral preference in *Drosophila*. Neuron *60*, 328–342.

Götz, K.G. (1964). Optomotorische Untersuchung des visuellen Systems einiger Augenmutanten der Fruchtfliege *Drosophila*. Kybernetik *2*, 77–92.

Haag, J., Wertz, A., and Borst, A. (2010). Central gating of fly optomotor response. Proc. Natl. Acad. Sci. USA *107*, 20104–20109.

Hassenstein, B., and Reichardt, W. (1956). Systemtheoretische Analyse der Zeit-, Reihenfolgen- und Vorzeichenauswertung bei der Bewegungsperzeption des Rüsselkäfers *Chlorophanus*. Z. Naturforsch. B *11*, 513–524.

Joesch, M., Plett, J., Borst, A., and Reiff, D.F. (2008). Response properties of motion-sensitive visual interneurons in the lobula plate of *Drosophila melanogaster*. Curr. Biol. *18*, 368–374.

Joesch, M., Schnell, B., Raghu, S.V., Reiff, D.F., and Borst, A. (2010). ON and OFF pathways in *Drosophila* motion vision. Nature *468*, 300–304.

Joesch, M., Weber, F., Eichner, H., and Borst, A. (2013). Functional specialization of parallel motion detection circuits in the fly. J. Neurosci. *33*, 902–905.

Jung, S.N., Borst, A., and Haag, J. (2011). Flight activity alters velocity tuning of fly motion-sensitive neurons. J. Neurosci. *31*, 9231–9237.

Kim, J.S., Greene, M.J., Zlateski, A., Lee, K., Richardson, M., Turaga, S.C., Purcaro, M., Balkam, M., Robinson, A., Behabadi, B.F., et al.; EyeWirers (2014). Space-time wiring specificity supports direction selectivity in the retina. Nature *509*, 331–336.

Kitamoto, T. (2001). Conditional modification of behavior in *Drosophila* by targeted expression of a temperature-sensitive *shibire* allele in defined neurons. J. Neurobiol. *47*, 81–92.

Land, M.F. (1997). Visual acuity in insects. Annu. Rev. Entomol. *42*, 147–177.

Maimon, G., Straw, A.D., and Dickinson, M.H. (2010). Active flight increases the gain of visual motion processing in *Drosophila*. Nat. Neurosci. *13*, 393–399.

Maisak, M.S., Haag, J., Ammer, G., Serbe, E., Meier, M., Leonhardt, A., Schilling, T., Bahl, A., Rubin, G.M., Nern, A., et al. (2013). A directional tuning map of *Drosophila* elementary motion detectors. Nature *500*, 212–216.

Masland, R.H. (2012). The neuronal organization of the retina. Neuron *76*, 266–280.

Mauss, A.S., Meier, M., Serbe, E., and Borst, A. (2014). Optogenetic and pharmacologic dissection of feedforward inhibition in *Drosophila* motion vision. J. Neurosci. *34*, 2254–2263.

Mauss, A.S., Pankova, K., Arenz, A., Nern, A., Rubin, G.M., and Borst, A. (2015). Neural circuit to integrate opposing motions in the visual field. Cell *162*, 351–362.

Meier, M., Serbe, E., Maisak, M.S., Haag, J., Dickson, B.J., and Borst, A. (2014). Neural circuit components of the *Drosophila* OFF motion vision pathway. Curr. Biol. *24*, 385–392.

Nern, A., Pfeiffer, B.D., and Rubin, G.M. (2015). Optimized tools for multicolor stochastic labeling reveal diverse stereotyped cell arrangements in the fly visual system. Proc. Natl. Acad. Sci. USA *112*, E2967–E2976.

Park, S.J.H., Kim, I.-J., Looger, L.L., Demb, J.B., and Borghuis, B.G. (2014). Excitatory synaptic inputs to mouse on-off direction-selective retinal ganglion cells lack direction tuning. J. Neurosci. *34*, 3976–3981.

Pfeiffer, B.D., Truman, J.W., and Rubin, G.M. (2012). Using translational enhancers to increase transgene expression in *Drosophila*. Proc. Natl. Acad. Sci. USA *109*, 6626–6631.

Reiff, D.F., Plett, J., Mank, M., Griesbeck, O., and Borst, A. (2010). Visualizing retinotopic half-wave rectified input to the motion detection circuitry of *Drosophila*. Nat. Neurosci. *13*, 973–978.

Rivera-Alba, M., Vitaladevuni, S.N., Mishchenko, Y., Lu, Z., Takemura, S.Y., Scheffer, L., Meinertzhagen, I.A., Chklovskii, D.B., and de Polavieja, G.G. (2011). Wiring economy and volume exclusion determine neuronal placement in the *Drosophila* brain. Curr. Biol. *21*, 2000–2005.

Schnell, B., Joesch, M., Forstner, F., Raghu, S.V., Otsuna, H., Ito, K., Borst, A., and Reiff, D.F. (2010). Processing of horizontal optic flow in three visual interneurons of the *Drosophila* brain. J. Neurophysiol. *103*, 1646–1657.

Schnell, B., Raghu, S.V., Nern, A., and Borst, A. (2012). Columnar cells necessary for motion responses of wide-field visual interneurons in *Drosophila*. J. Comp. Physiol. A Neuroethol. Sens. Neural Behav. Physiol. *198*, 389–395.

Schnell, B., Weir, P.T., Roth, E., Fairhall, A.L., and Dickinson, M.H. (2014). Cellular mechanisms for integral feedback in visually guided behavior. Proc. Natl. Acad. Sci. USA *111*, 5700–5705.

Shinomiya, K., Karuppudurai, T., Lin, T.Y., Lu, Z., Lee, C.H., and Meinertzhagen, I.A. (2014). Candidate neural substrates for off-edge motion detection in *Drosophila*. Curr. Biol. *24*, 1062–1070.

Silies, M., Gohl, D.M., Fisher, Y.E., Freifeld, L., Clark, D.A., and Clandinin, T.R. (2013). Modular use of peripheral input channels tunes motion-detecting circuitry. Neuron *79*, 111–127.

Sponberg, S., Dyhr, J.P., Hall, R.W., and Daniel, T.L. (2015). Insect Flight: luminance-dependent visual processing enables moth flight in low light. Science *348*, 1245–1248.

Strother, J.A., Nern, A., and Reiser, M.B. (2014). Direct observation of ON and OFF pathways in the *Drosophila* visual system. Curr. Biol. *24*, 976–983.

Takemura, S.Y., Karuppudurai, T., Ting, C.-Y., Lu, Z., Lee, C.-H., and Meinertzhagen, I.A. (2011). Cholinergic circuits integrate neighboring visual signals in a *Drosophila* motion detection pathway. Curr. Biol. *21*, 2077–2084.

Takemura, S.Y., Bharioke, A., Lu, Z., Nern, A., Vitaladevuni, S., Rivlin, P.K., Katz, W.T., Olbris, D.J., Plaza, S.M., Winston, P., et al. (2013). A visual motion detection circuit suggested by *Drosophila* connectomics. Nature *500*, 175–181.

Tuthill, J.C., Nern, A., Holtz, S.L., Rubin, G.M., and Reiser, M.B. (2013). Contributions of the 12 neuron classes in the fly lamina to motion vision. Neuron *79*, 128–140.

Wardill, T.J., List, O., Li, X., Dongre, S., McCulloch, M., Ting, C.-Y., O'Kane, C.J., Tang, S., Lee, C.-H., Hardie, R.C., and Juusola, M. (2012). Multiple spectral inputs improve motion discrimination in the *Drosophila* visual system. Science *336*, 925–931.

Werblin, F.S., and Dowling, J.E. (1969). Organization of the retina of the mudpuppy, *Necturus maculosus.* II. Intracellular recording. J. Neurophysiol. *32*, 339–355.

Yonehara, K., Farrow, K., Ghanem, A., Hillier, D., Balint, K., Teixeira, M., Jüttner, J., Noda, M., Neve, R.L., Conzelmann, K.-K., and Roska, B. (2013). The first stage of cardinal direction selectivity is localized to the dendrites of retinal ganglion cells. Neuron *79*, 1078–1085.